International Journal of Biological Macromolecules 359 (2026) 151809

Contents lists available at ScienceDirect

International Journal of Biological Macromolecules

journal homepage: www.elsevier.com/locate/ijbiomac

Tailoring alkyl modification patterns in hyaluronic acid derivatives serving as carriers for enhanced kartogenin delivery and chondrogenic responses

Magdalena Wytrwal [a,*,1], Sylwia Rzepa [a,1], Ewa Ocłoń [b], Mirosław Kucharski [c], Ewelina Bik [a], Katarzyna Filipek [a], Wendy Koevoet [d], Gerjo J.V.M. van Osch [d,e,f], Szczepan Zapotoczny [g]

[a] Academic Centre for Materials and Nanotechnology, AGH University of Krakow, Mickiewicza 30, 30-059, Krakow, Poland
[b] Laboratory of Recombinant Proteins Production, University of Agriculture in Krakow, 1C Redzina Street, 30-248, Krakow, Poland
[c] Department of Animal Physiology and Endocrinology, University of Agriculture in Krakow, al. A Mickiewicza 24/28, 30-059, Krakow, Poland
[d] Department of Otorhinolaryngology, Head and Neck Surgery, Erasmus MC, University Medical Center, Rotterdam, the Netherlands
[e] Department of Orthopaedics and Sports Medicine, Erasmus MC, University Medical Center, Rotterdam, the Netherlands
[f] Department of Biomechanical Engineering, Faculty of Engineering, University of Technology Delft, the Netherlands
[g] Faculty of Chemistry, Jagiellonian University, Gronostajowa 2, 30-387, Krakow, Poland

ARTICLE INFO

Keywords:
Amphiphilic hyaluronic acid
Kartogenin
Drug delivery systems
Critical aggregation concentration
Cartilage

ABSTRACT

Cartilage diseases often worsen with age and require orthopedic treatment. To reduce the need for surgery, developing new methods and biomaterials to stimulate and support cartilage regeneration is essential. Among the most promising options are drug delivery systems based on hyaluronic acid (HA), a natural component of the extracellular matrix, known for its biocompatibility, biodegradability, and adjustable chemical modification. In this study, we systematically tailored alkyl modification patterns in HA by introducing alkyl chains of varying lengths and degrees of substitution. Following comprehensive physicochemical characterization, the resulting amphiphilic derivatives formed polyelectrolyte aggregates suitable for controlled delivery of bioactive molecules. Kartogenin (KGN), a small, moderately hydrophobic molecule with chondroprotective effects, was used as a model drug to test the system's potential. The engineered HA derivatives efficiently encapsulated KGN, and specific formulations promoted chondrogenesis in both 2D and 3D cultures by upregulating key chondrogenic markers. These findings highlight the importance of precise alkyl pattern design in modulating HA-based carrier behavior and pave the way for further optimization, including refined substitution strategies, ligand conjugation approaches, and expanded biocompatibility studies toward future in vivo applications.

1. Introduction

Joint diseases encompass a broad range of conditions that impair synovial joints - structures connecting bones and enabling movement. They arise from inflammatory, degenerative, autoimmune, infectious, or mechanical causes. Major types include osteoarthritis (OA), rheumatoid arthritis (RA), gout, ankylosing spondylitis (AS), and psoriatic arthritis (PsA). Cartilage degeneration increases with age, posing a major orthopedic challenge. In 2020, about 14.8% of people over 30 (≈595 million globally) had OA, a number projected to reach nearly 1 billion by 2050 due to aging and obesity [1]. To reduce the need for surgical interventions, effective cartilage regeneration strategies are needed [2]. Current options – such as autologous chondrocyte implantation, joint lavage, mesenchymal stem cells and their vesicles, platelet-rich plasma, and injections of glycosaminoglycans like chondroitin sulfate or hyaluronic acid (HA) – offer temporary relief [3–5]. Although these strategies offer initial benefits, they do not support long-term cartilage regeneration [6]. Thus, developing improved or novel strategy to protect and regenerate cartilage remains a critical goal.

Natural biopolymers, such as polysaccharides, are vital for cartilage repair and regeneration due to their biocompatibility, biodegradability, and non-toxicity. They can act as scaffolds for cell growth, carriers for controlled drug delivery, and bioactive agents that modulate the cellular environment to promote tissue healing [7]. Their natural abundance and low production cost further enhance their biomedical potential. Most polysaccharides possess hydrophilic functional groups (hydroxyl,

* Corresponding author at: AGH University of Krakow, Academic Centre for Materials and Nanotechnology, al. A. Mickiewicza 30, 30-059, Krakow, Poland.
E-mail address: wytrwal@agh.edu.pl (M. Wytrwal).
[1] Equally contributed

https://doi.org/10.1016/j.ijbiomac.2026.151809
Received 5 December 2025; Received in revised form 27 March 2026; Accepted 1 April 2026
Available online 3 April 2026

carboxyl, amino) that enable non-covalent interactions with biological tissues [8–10]. Hydrogen bonding, electrostatic interactions, and van der Waals forces drive their self-assembly. Among these, HA is one of the most studied biopolymers. HA, a glycosaminoglycan, is abundant in cartilage, skin, and synovial fluid (3–6 MDa; 2.4–4.0 mg/mL) [11]. It is degraded by hyaluronidases - enzymes involved in various physiological and pathological processes that increase tissue permeability and reduce fluid viscosity [12,13].

Biodegradable nanocarriers based on polymers such as HA often exhibit limited chemical and physical stability in aqueous environments, resulting in hydrolysis, drug leakage, or aggregation [14]. To address these issues, HA derivatives have been developed to enhance hydrolytic and enzymatic resistance while stabilizing carrier systems [15]. Alkyl modification of HA is an effective strategy to improve these properties. Such derivatives can coat liposomes to provide controlled drug release and improved stability [16], or form oil-core nanocapsules as efficient drug carriers [17]. Payne et al. demonstrated that amphiphilic HA conjugates (*n*-hexyl, *n*-dodecyl, and *n*-octadecyl) spontaneously adopt random coil structures through hydrophobic collapse, with the longest alkyl chains producing the most compact and ordered conformations [18]. The introduction of hydrophobic moieties not only improves the viscoelastic and rheological properties of HA but also increases its enzymatic resistance. In cartilage-related applications, these effects translate into enhanced viscoelastic behavior and the inhibition of matrix metalloproteinases (MMP13 and MMP8) activity, as observed in osteoarthritis patients [11,12,19].

Among bioactive compounds for cartilage regeneration, kartogenin (KGN) is a promising small molecule that promotes chondrogenic differentiation of mesenchymal stem cells and protects cartilage and subchondral bone [20]. However, its moderate hydrophobicity causes rapid systemic clearance. To improve its stability and effectiveness, various delivery systems, such as liposomes [21], exosomes [22], micelles [23], and hydrogels [24,25], have been studied. Kang et al. developed HA-based hydrogels containing covalently attached micelles of PEGylated KGN [26]. Tikakosol et al. tested hydrogels composed of *N*-succinyl chitosan and hyaluronic dialdehyde loaded with KGN [27]. Li et al. showed the hydrazone/covalent dual-crosslinked HA hydrogel with KGN-loaded poly(lactic-*co*-glycolic acid) microspheres [28]. Given the above and the diversity of possible modifications, it is essential to conduct stepwise investigations into how subtle structural changes influence the performance of the designed carrier or matrix.

While alkyl-modified HA and KGN delivery systems have been previously reported, the novelty of this study lies in the systematic variation of alkyl chain length and degree(s) of substitution (DS) within a unified HA-based platform. This approach enables direct correlation of subtle structural changes with aggregation behavior, drug binding and release, cytotoxicity, and chondrogenic response. Notably, these properties do not evolve linearly with alkyl chain length or substitution degree, underscoring the need for systematic investigation. Overall, the study provides a structure-property-function framework, rather than focusing on a single optimized formulation. We hypothesized that tailoring alkyl modification patterns in HA derivatives would enable their self-assembly into stable, biocompatible nanocarriers capable of efficiently encapsulating KGN, controlling its release, and enhancing its chondrogenic activity in human mesenchymal stem cells. To test this concept, HA was systematically modified with alkyl chains ranging from *n*-hexyl to *n*-octadecyl at varying degrees of substitution and thoroughly characterized by spectroscopic techniques. The resulting amphiphilic derivatives formed nanometer-scale micelles with hydrophobic cores suitable for KGN loading. Their physicochemical properties – including critical aggregation concentration (CAC), encapsulation efficiency, and colloidal stability - were evaluated using DLS, ζ-potential, and fluorescence spectroscopy, with selected systems further examined by cryo-TEM. Biological performance was assessed in both 2D and 3D hUC-MSC cultures. Collectively, these findings demonstrate that precisely tuned alkylated HA derivatives represent promising nanocarriers for hydrophobic agents, supporting their potential application in cartilage regeneration.

2. Materials and methods

2.1. Synthesis of alkylated hyaluronates (HACx)

HA from *Streptococcus equi* subsp. *Zooepidemicus* (Nutrihyl, HA) was obtained from Contipro (Dolní Dobrouč, Czech Republic). The manufacturer characterized this product as having a weight-average molar mass (M_w) of 280,000 Da and a number-average molar mass (M_n) of 172,000 Da; the M_w/M_n ratio (molar mass dispersion) was 1.629 (using SEC-MALS analysis); and the purity was 96.9%. The synthesis of alkylated derivatives of HA was carried out following the previously described procedure (see SI for details) [29]. As a result, six derivatives (HACx) were obtained: HAC6L (HA modified with 1-hexylamine with a lower DS - L), HAC12L (1-dodecylamine, lower DS - L), HAC16L (1-hexadecylamine, lower DS - L), HAC16H (1-hexadecylamine, higher DS - H), HAC18L (1-octadecylamine, lower DS - L), and HAC18H (1-octadecylamine, higher DS - H). The DS were determined semi-quantitatively from ^{1}H NMR and quantitatively from XPS spectra (Tab. S1 and S2). ^{1}H NMR spectra were recorded using a Bruker Avance III HD 400 MHz spectrometer (Bruker, Ettlingen, Germany) at a temperature of 80 °C. Samples were prepared by dissolving 10 mg of polymers in a D_2O:DMSO-d_6 mixture (4:1; v/v). Moreover, extra analysis of ^{1}H NMR spectra was performed in DMSO-d_6:D_2O mixture (7:1; v/v) to visualize the hydrophobization of HA better. A Versa Probe II system (ULVAC-PHI, Chigasaki, Japan) with a microfocused (100 μm, 25 W) Al Kα X-ray beam was used for XPS analysis. The photoelectron spectra were collected from 300 μm^2 areas with an analyzer pass energy of 46.95 eV and a take-off angle of 45°. Charging effects were compensated with a dual-beam charge neutralizer. The chamber pressure was maintained below 5×10^{-7} Pa. All XPS peaks were calibrated to C 1 s peak at 285.0 eV for C—C bonds. Spectrum background subtraction was performed using the Shirley method. Elemental compositions were calculated with PHI MultiPak™ software (version 9.9.2). Additionally, the changes in DS were checked by ATR-FTIR spectra. ATR-FTIR spectra were recorded on a Bruker Tensor II spectrometer (Bruker Optics GmbH & Co. KG, Ettlingen, Germany) over the range of 350–4000 cm^{-1}, with powder samples deposited onto a diamond crystal.

2.2. Critical aggregation concentration (CAC) assay

The CACs of the HA, HACx polyanions in PBS were determined using fluorescence techniques following the procedure previously described [30]. Additionally, the apparent CACs of physical mixtures of HA with 1-octadecylamine at 2% and 10% (corresponding to determined DSs) were measured. In brief, a series of samples with different concentrations (0–8 mg/mL) and a fixed concentration of 4 μM 1,6-diphenyl-1,3,5-hexatriene (DPH, Sigma-Aldrich, Darmstadt, Germany), a fluorescent probe, were prepared and stirred for 4 h in the dark. Afterward, their fluorescence spectra ($\lambda_{exc} = 350$ nm) were recorded and the fluorescence intensities at maximum were plotted against the polymer concentration. Fluorescence emission spectra were obtained with an Edinburgh Instruments FS5 spectrometer (Livingston, Scotland, United Kingdom).

2.3. Encapsulation of KGN in aggregates of the HA derivatives

The encapsulation of KGN in HACx-based aggregates was studied by titrating 10 mL (2 mg/mL) polymer solutions in PBS with a 1 mM KGN solution in tetrahydrofuran (THF, >99.0%, Sigma-Aldrich, Darmstadt, Germany) (doses: 4 × 25 μL, 4 × 50 μL, 4 × 100 μL). First, the KGN dose was added to the polymer solution and stirred for 2 min under an inert gas flow to evaporate THF. Then, after each addition of KGN, fluorescence spectra of the solutions were recorded (λ_{exc} = 290 nm). The

apparent dissociation constants (K_d) were determined through hyperbolic curve fitting using the following equation (Eq. (1)):

$$y = (B_{max} \times X)/(K_d + X) \quad (1)$$

where: K_d is defined as the concentration of ligand X (KGN) at which half of the maximum binding is achieved – that is, when $y = B_{max}/2$ (the amount of KGN needed to reach half-maximum partitioning between the aqueous and hydrophobic phases at equilibrium); B_{max} - maximum fluorescence intensity at $\lambda_{em} = 380$ nm [31]. The association constant (K_a) was calculated as the reciprocal of K_d ($K_d = 1/K_a$).

Moreover, the size changes of HACx and HACx-KGN were analyzed using Dynamic Light Scattering (DLS) measurements, performed at 25 °C with a Malvern Zetasizer Nano ZS (Malvern Panalytical Ltd., Worcestershire, United Kingdom) operating at a 173° detection angle. 2 mg/mL of polymeric aggregates in PBS were analyzed using standard DLS cuvettes.

2.4. Cryo-TEM studies

Cryogenic transmission electron microscopy (Cryo-TEM) was performed using a Glacios transmission electron microscope (Thermo Fisher Scientific, Waltham, USA) equipped with a Falcon 4 direct electron detector (Thermo Fisher Scientific, Waltham, USA). Micrographs were acquired at a nominal magnification of 11,800×, corresponding to a calibrated pixel size of 2.08 Å per pixel. The EPU analyzed the collected data - Automated Data Acquisition Software (Thermo Fisher Scientific, Waltham, USA). Before use, the grids with a holey carbon film (Quantifoil R 2/1 Cu 200 mesh grids, Quantifoil Micro Tools GmbH, Germany) were glow-discharged at 14 mA for 5 s. Samples (2 mg/mL of solutions of HAC18L, HAC18L-KGN, and HAC12L-KGN in PBS) were vitrified in liquid ethane using a Vitrobot Mark IV (Thermo Fisher Scientific, Waltham, USA) operated at 4 °C and 95% relative humidity. Blotting was performed with a blot force of 4, a blot time of 2 s, a wait time of 10 s, and one blot cycle. After preparation, the vitrified specimens were kept under liquid nitrogen until measurement.

2.5. Release of KGN from the HACx-based aggregates

As a first step, the Pur-A-Lyzer™ (Midi Dialysis Kit, MWCO 3.5 kDa (Sigma-Aldrich, Darmstadt, Germany) was filled with 0.8 mL of ultrapure water and incubated for 5 min. Then, the tubes were emptied and checked for water leakage. Next, 800 μL of the dispersion of HACx-based aggregates (2 mg/mL) containing encapsulated KGN (HACx-KGN) at a concentration of 0.1 mM were loaded into the Pur-A-Lyzer tubes, which were sealed with the caps provided by the manufacturer. Each tube was placed in a separate container with 17 mL of PBS and stirred with a magnetic stirrer to maintain consistent conditions for the KGN release. During dialysis, the fluorescence of the released KGN into the PBS solution (outside the tubes) was measured at several time points (1, 2, 3, 5, 6, 8, 14, 24 h). Additionally, fluorescence of KGN ($\lambda_{exc} = 290$ nm) was left in the starting dispersions after 80 h and again after 6 days (144 h) of continuous dialysis. The maximum emission wavelength of KGN fluorescence was 350 nm. To analyze the fluorescence intensity data of KGN released from the aggregates, the Weibull function based on the three-parameter Weibull model was used (Eq. (2)):

$$y(t) = A \bullet \left(1 - exp\left(-\left(\frac{t}{\alpha}\right)^{\beta}\right)\right) \quad (2)$$

where: y(t) represents the fluorescence intensity at a specific time, A is an asymptotic value (upper limit), α is the scale-related time constant, and β is the shape parameter that describes the release mechanism [32]. The Weibull fit was generated using the nonlinear curve-fitting module in OriginPro 2023b (version 10.0.5.157, OriginLab Corporation, Northampton, USA).

2.6. Cell culture

Primary human umbilical cord mesenchymal stem cells (hUC-MSCs) were obtained from PromoCell (Cat. No. C-12971, Heidelberg, Germany), derived from a single donor as indicated by the manufacturer. The hUC-MSCs were isolated, characterized, and verified to be multipotent. All cellular experiments were performed on passages 2–4. Depending on the experimental design, the cells were cultured either in 2D monolayer systems or as 3D pellets.

2.6.1. Induction of chondrogenic differentiation of hUC-MSCs in 2D cell culture

hUC-MSCs were cultured in Dulbecco's Modified Eagle's Medium (DMEM/F12, Sigma-Aldrich, Darmstadt, Germany), supplemented with penicillin, streptomycin, and 2% heat-inactivated FBS. Cells were seeded in 24-well plates at a density of 1.5×10^4 cells per well. After 24 h, the culture medium was replaced with fresh medium (control) or medium containing selected non-toxic concentrations of HACx and HACx-KGN aggregates, each in triplicate. The cells were cultured for 24 h under continuous stimulation with HACx and HACx-KGN to evaluate early gene expression changes associated with chondrogenic differentiation. Additionally, cells were stimulated for 24 h with free KGN as a control. The applied KGN concentrations corresponded exactly to the amounts present in the respective polymer aggregates and ranged from 0.25 to 0.5 μM. Free KGN was dissolved in DMSO, and equivalent solvent concentrations were used in control conditions to exclude solvent-related effects.

Total RNA was extracted using the Gene MATRIX Universal RNA Purification Kit (EURx, Gdansk, Poland), and 0.5 μg of RNA was reverse-transcribed into cDNA using the High-Capacity cDNA Reverse Transcription Kit (Thermo Fisher Scientific, Waltham, USA). Quantitative PCR was conducted with PowerUp™ SYBR™ Green Master Mix on a StepOnePlus™ Real-Time PCR System (Thermo Fisher Scientific, Waltham, USA) to measure the expression of SRY-box transcription factor 9 (*SOX9*), aggrecan (*ACAN*), collagen type II alpha 1 chain (*COL2A1*), and collagen type I alpha 1 chain (*COL1A1*). Gene expression levels were normalized using the geometric mean of two internal control genes, glyceraldehyde-3-phosphate dehydrogenase (*GAPDH*) and 18S ribosomal RNA (*18S rRNA*). Gene stability was evaluated using the geNorm algorithm, and both genes showed high expression stability ($M < 0.5$), supporting their use as suitable internal controls. Primers were designed using Primer Express software based on NCBI sequences (Tab. S3) and synthesized by Genomed (Warsaw, Poland).

2.6.2. Cytotoxicity assay

Cell viability was evaluated using the MTT assay. hUC-MSCs were seeded in 96-well plates at a density of 3.0×10^4 cells/cm^2. After 24 h, the culture medium was replaced with either control medium or medium containing increasing concentrations of polymers in the form of free HACx and HACx-KGN aggregates (0.5–200 μg/mL). After another 24 h incubation, MTT solution (Sigma-Aldrich, Darmstadt, Germany) was added, and cells were incubated for 4 h. The resulting formazan crystals were dissolved in 2-propanol (96%, p.a., POCH, Gliwice, Poland), and the absorbance of the solutions was measured at 562 nm using a microplate reader (Infinite M Nano, Tecan, Männedorf, Switzerland). All experiments were performed in triplicate and repeated three times independently. The IC_{50} value was defined as the polymer concentration that reduced cell viability by 50% compared to the untreated control.

2.6.3. Induction of chondrogenic differentiation of hUC-MSCs in 3D cell culture

hUC-MSCs were cultured in 3D pellets following the previous protocol [33]. Briefly, 2×10^5 hUC-MSCs were centrifuged at 1100 rpm for 8 min in polypropylene tubes. To induce chondrogenesis, a different chondrogenic medium was used, reflecting the transition from

monolayer expansion to pellet-based differentiation. The pellets were cultured in medium containing DMEM GlutaMAX (Gibco, Waltham, USA), 1% ITS+ Premix (Corning, New York, USA), Antibiotic-Antimycotic Solution (100 IU/mL penicillin, 10 μg/mL streptomycin, 0.25 μg/mL amphotericin B, Sigma-Aldrich, Darmstadt, Germany), 1 mM sodium pyruvate (Sigma-Aldrich, Darmstadt, Germany), 40 μg/mL proline (Sigma-Aldrich, Darmstadt, Germany), and 0.1 mM freshly added AA2P (Sigma-Aldrich, Darmstadt, Germany), with 100 nM dexamethasone (Sigma-Aldrich, Darmstadt, Germany). TGF-β1 (2 ng/mL; R&D Systems, Minneapolis, USA) was added depending on the experimental condition. After 24 h, the medium was replaced with fresh chondrogenic medium with or without 2 ng/mL TGF-β1, as indicated. The medium was refreshed twice weekly for 3 weeks. Each time, the fresh HACx and HACx-KGN were prepared at a concentration of 7.5 μg/mL. After 3 weeks, spheroids were harvested on ice. RNA isolation was performed using a guanidinium thiocyanate-phenol-chloroform extraction method, also known as the Chomczynski and Sacchi method, with TRI Reagent® (Sigma-Aldrich, Darmstadt, Germany) [34]. In the first step, each spheroid was disrupted with a pestle in TRI Reagent®. The RT-PCR procedures were carried out according to paragraph 2.6.1.

2.7. Alcian Blue and Fast Green staining

hUC-MSCs were seeded onto Nunc™ Lab-Tek™ Chamber Slide System (Thermo Fisher Scientific, USA) at a density of 2×10^4 cells per well in DMEM/F12 supplemented with 2% FBS. Cells were stimulated with HAC12L-KGN and HAC16L-KGN at the concentrations of 25 μg/mL for 7 days. Following treatment, cells were fixed with 4% paraformaldehyde (PFA) for 15 min at room temperature, washed three times with PBS and once with distilled water. For Alcian Blue staining, cell monolayers were incubated in 3% acetic acid for 4 min and subsequently stained with 1% Alcian Blue solution (8GX; BLD Pharmatech Ltd., Shanghai, China) for 1 h at room temperature. After staining, samples were rinsed with 3% acetic acid and washed four times with distilled water. For Fast Green staining, after fixation and washing, cells were incubated in 1% acetic acid for 2 min and then stained with 1% Fast Green solution (BLD Pharmatech Ltd., Shanghai, China) for 1 h at room temperature, followed by washing with 1% acetic acid and four rinses with distilled water. Finally, samples were mounted using Fluoromount-G (Thermo Fisher Scientific, Waltham, MA, USA). Images were acquired using an Olympus microscope equipped with an Olympus digital camera and cellSens Entry software (Olympus Corporation, Tokyo, Japan).

2.8. Statistical analysis

The individual gene expression level was calculated using relative quantitative (RQ) analysis and the Pfaffl model, which accounted for reaction efficiency for each gene [35]. The normality of the gene expression distribution for all analyzed variables was assessed with the Shapiro-Wilk test. A one-way analysis of variance (ANOVA) was used to compare the experimental groups. Significant differences between the groups were determined using Tukey-Kramer HSD post hoc test in Statistica ver. 10 (StatSoft Inc., Tulsa, USA). Changes in target gene expression are shown as the ratio of treated cells to untreated cells. Data are presented as the mean fold change. Statistical differences in cell viability (MTT assay) between polymer-only and polymer-KGN groups at each concentration were assessed using unpaired two-tailed Student's *t*-tests, followed by Holm–Bonferroni correction for multiple comparisons.

3. Results and discussion

The results demonstrate that even small variations in alkyl chain length and DS markedly influence both the self-assembly behavior and biological performance of HA-based carriers. Systematic comparison across the HACx series reveals clear structure-dependent trends in aggregation characteristics, drug binding affinity, release kinetics, cytotoxicity, and chondrogenic response. Crucially, these effects follow non-linear trends, indicating the presence of optimal hydrophobic modification windows rather than monotonic improvement with increasing alkyl chain length.

3.1. Characterization of hyaluronic acid derivatives

Based on the reaction scheme shown in Fig. 1, six HA derivatives with varying alkyl chain lengths and DS were successfully synthesized: HAC6L, HAC12L, HAC16L, HAC18L, HAC16H, and HAC18H (see SI for details). The resulting derivatives were analyzed using various spectroscopic techniques, including ^{1}H NMR, IR, and XPS, to determine their chemical structures.

The ^{1}H NMR spectra (measured in D_2O/DMSO-d_6 mixture, 4:1, v/v) of each derivative and substrate, along with selected signals assigned to the relevant protons, are shown in Fig. S1. The integration of protons from the acetyl group (HN-C(O)-C$\underline{H_3}$) (δ = 1.83 ppm) was fixed and set to 3H. The integration of methylene groups in substituted alkyl chains (HN-CH_2-CH_2-(C$\underline{H_2}$)$_y$-CH_3) (δ = 1.21 ppm) was used to calculate the DS by NMR technique (Table 1 and Table S1).

There are numerous reports in the literature describing the acquisition of NMR spectra of amphiphilic HA derivatives in pure DMSO-d_6 to determine the DS with hydrophobic fragments [18,36]. Since recording NMR spectra of amphiphilic derivatives is often challenging and the use of solvent mixtures remains somewhat controversial, we also attempted such measurements for our derivatives. The solubility of HA and HACx polymers in DMSO-d_6 alone is very low; therefore, a small amount of D_2O (DMSO-d_6:D_2O = 7:1, *v*/v) was added. The spectra were recorded at 80 °C, and the results are presented in Fig. S2. The presence of alkyl fragments was confirmed based on the following characteristic signals: 0.82 ppm (C**H₃**–$(CH_2)_\gamma$–CH_2–CH_2–NH–), 1.21 ppm (CH_3–(C**H₂**)$_\gamma$–CH_2–CH_2–NH–), 1.47 ppm (CH_3–$(CH_2)_\gamma$–C**H₂**–CH_2–NH–), and 2.69 ppm (CH_3–$(CH_2)_\gamma$–CH_2–C**H₂**–NH–). The last two signals were observed only for HAC16 and HAC18. The signal integration was normalized to 3H, corresponding to the acetyl group (HN-C(O)-C**$\underline{H_3}$**) (δ = 1.83 ppm). The apparent DS calculated from NMR spectra (HAC6L – ~9.5%; HAC12L – ~11.4%; HAC16L – ~60%; HAC16H – ~103%; HAC18L – ~83%; HAC18H – ~119%) were markedly higher than expected (Tab. S1). This overestimation likely results from reverse micelle formation, in which hydrophobic chains are exposed, and the HA backbone is shielded. NMR analysis does not provide unambiguous results due to the limited mobility of the alkyl groups in these amphiphilic HA derivatives, particularly the absence of the key proton signal confirming covalent attachment, necessitating the use of alternative methods.

XPS spectra were collected to analyze the contribution of specific carbon bonds in the substrate and its derivatives (Fig. S3). A clear increase in the contribution of the C—C bond at 285.0 eV is observed between HA and its derivatives (Tab. S2). Alkyl substitution does not affect the contribution of C-O-C bonds at 286.2 eV, which is why DS was calculated from the atomic concentration of C—C and C-O-C (Tab. S2). Both DS analysis methods – XPS and ^{1}H NMR in D_2O:DMSO-d_6, 4:1 – show a reasonable correlation, and the corresponding values are summarized in Table 1. For derivatives with lower substitution levels, the alkyl content is close to 2%, whereas higher DS of approximately 5% for HAC16H and 11% for HAC18H are observed based on XPS analysis. DS values obtained from ^{1}H NMR reflect the aggregation- and solvent-dependent nature of measurements in amphiphilic polyelectrolyte systems. Variations in solvent composition affect alkyl chain mobility and signal integration, rendering NMR-derived DS values apparent rather than strictly quantitative. Accordingly, XPS-derived DS values provide a more reliable basis for interpreting the structure-property-function relationships discussed below. Additionally, IR spectra confirmed the effective derivatization of HA by the alkyl chains as evidenced by increased C—H stretching vibrations at 2980, 2920, and 2850 cm^{-1} (Fig. S4).

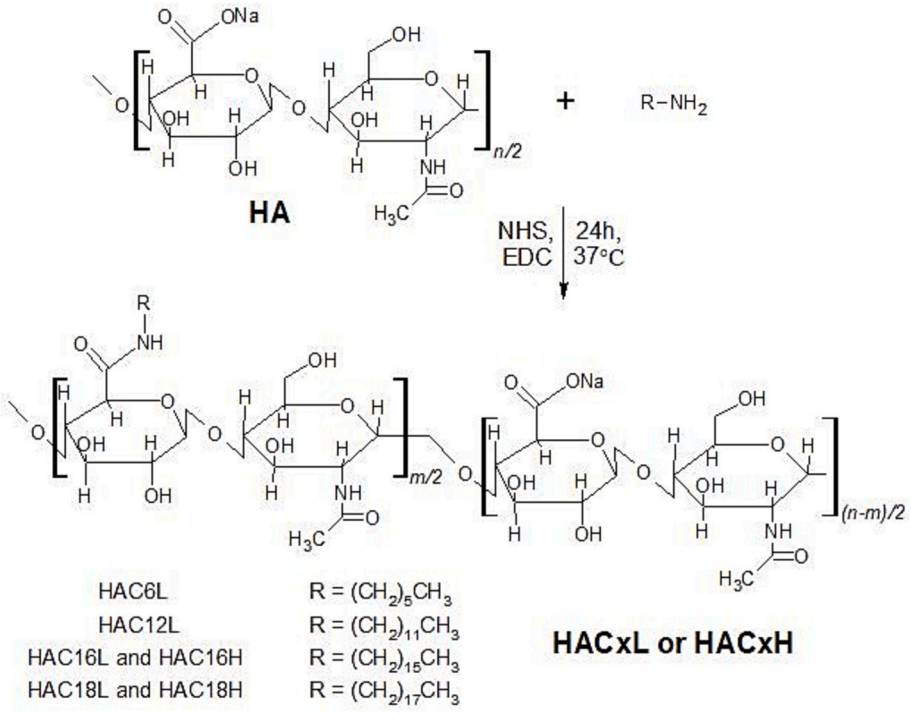

Fig. 1. Scheme of structural modification of HA with alkyl chains.

Table 1
Comparison of apparent DS values derived from ^{1}H NMR (semi-quantitative, spectra measured in D_2O/DMSO-d_6 mixture, 4:1, *v*/v) and DS values obtained from XPS (quantitative), together with the corresponding critical aggregation concentrations (CAC).

Polymer	DS (%)		CAC (mg/mL)
	^{1}H NMR	XPS	
	apparent[a]	quantitative	
HAC6L	~3.5	~2.4	1.56 ± 0.15
HAC12L	~1.5	~2.8	0.92 ± 0.16
HAC16L	~5.5	~2.7	0.22 ± 0.04
HAC18L	~2.2	~2.0	0.09 ± 0.01
HAC16H	~6.8	~4.8	0.05 ± 0.01
HAC18H	~12.5	~11.5	0.06 ± 0.01

[a] ^{1}H NMR-derived DS values represent apparent, semi-quantitative estimates influenced by aggregation effects and solvent-dependent chain mobility.

The hydrophobically modified GAGs, dispersed in an aqueous medium, spontaneously assemble into nanometric micelle-like structures with polysaccharide chains forming the shells and hydrophobic groups forming the cores [30]. The hydrophobic core can trap water-insoluble drugs and release them through various mechanisms. The ability of HA and HACx to self-organize into micelle-like structures was examined using the common fluorescence method with 1,6-diphenyl-1,3,5-hexatriene (DPH) as a molecular probe [37]. DPH fluorescence increases significantly above the critical micellar concentration (CMC) due to its penetration into the hydrophobic interior of the micelles. In this study, the term CAC is used instead of CMC, because the investigated HA derivatives are amphiphilic polyelectrolytes whose self-assembly occurs through gradual formation of dynamic, pseudo-micellar aggregates rather than classical micelles. The compactness of these hydrophobic domains, governed by alkyl chain length and DS, directly affects drug binding, release behavior, and cytotoxicity. The dependence of DPH fluorescence intensity on polymer concentration (ranging from 0 to 8.0 mg/mL) was analyzed. Fig. 2 displays the differences in self-aggregation between HA and its derivatives.

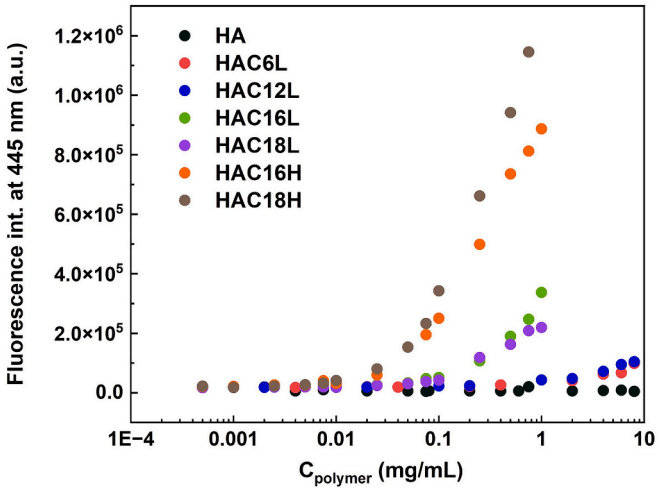

Fig. 2. The fluorescence intensity of DPH probe (C_{DPH} = 4 μM, λ_{ex} = 350 nm) at 445 nm as a function of the concentration of HA and HACx.

HA, the parent polymer without hydrophobic chains, did not self-assemble into micelle-like structures. For HACx derivatives, DPH fluorescence was highly dependent on polymer concentration, alkyl chain length, and the DS. The best-fit trend lines are shown in Fig. S5. The CAC values were derived from the intersection points and summarized in Table 1. Results confirmed that increasing alkyl chain length and DS promote the spontaneous formation of pseudo-micelles at lower polymer concentrations. Our previous study on chondroitin sulfate substituted with *n*-octadecyl groups also demonstrated this tendency to aggregate into pseudo-micelles with higher DS [30]. Furthermore, to compare the chemical modification of HA with the physical mixture of HA and 1-octadecylamine, additional CAC measurements were performed for the physical mixture containing 1-octadecylamine at 2% and 10% corresponding to the determined DS as HAC18L and HAC18H (Fig. S6). The results are presented on both logarithmic and linear scales

to better illustrate the differences between the two tested systems. For the HAC18L and HAC18H, the aggregation started at approximately 0.09 mg/mL and 0.06 mg/mL, respectively. In the case of the physical mixture of HA + 2% or HA + 10% 1-octadecylamine, the increase in fluorescence intensity of the DPH probe started at a much higher concentration, approximately 0.17 mg/mL, and was much milder compared to the systems with the synthesized amphiphilic polymers. These results clearly indicate that chemical grafting of hydrophobic chains onto the HA backbone significantly lowers the CAC compared to physical mixtures, confirming the more efficient and stable self-assembly of the chemically modified polymers. Moreover, the CAC of chemically modified HA depends strongly on DS, as the hydrophobic domains suitable for solubilization of DPH probe are formed at lower polymer concentration if the DS value is higher. Such observations indirectly indicate covalent attachment of the alkyl chains to the polymer backbone in the synthesized HA derivatives.

3.2. Interactions of polyanions with KGN

The procedure for incorporating KGN into HACx is shown schematically in Fig. 3A. Fluorescence spectroscopy was employed as a comparative approach to evaluate KGN association with HACx polymer aggregates under identical experimental conditions. KGN was integrated into HACx aggregates at concentrations several times higher than their CAC values (2 mg/mL). Fluorescence spectra of KGN were measured, with a maximum emission at 380 nm, as shown in Fig. 3B. Fluorescence intensity increases as KGN concentration rises, though with diminishing returns, indicating saturation behavior. KGN in pure PBS and in the presence of HA exhibits much higher fluorescence than in the presence of HACx aggregates. However, KGN, as a hydrophobic compound (lipophilicity parameter log $P = 3.8 \pm 0.4$, predicted using ACD/Labs software version 2020.2.1), can incorporate into the hydrophobic core of carriers while also existing in equilibrium with a polar environment [38]. Among HACx samples, the intensity varies slightly, suggesting differences based on the type of hydrophobization. This effect could be caused by fluorescence quenching due to the local environment or the self-quenching phenomenon of KGN, or other π–π interactions or dipole–dipole interactions with the polymer [39].

Hyperbolic curves were fitted to the KGN saturation binding curves as described in the experimental section. The coefficients K_d and K_a were calculated based on this fitting (Table 2), which are respectively defined as the amount of substance needed to fill half of the space in the created system and the ease of encapsulation of the active substance inside the system [31]. The resulting apparent binding parameters (K_d and K_a) provide a semi-quantitative description of KGN affinity for different HACx assemblies, with lower K_d and higher K_a indicating greater partitioning of KGN into hydrophobic domains within the aggregates. The K_d coefficients for the control samples (KGN in PBS and KGN in HA) are the highest, while the K_a values are the lowest compared to our polymeric systems. Conversely, the lowest K_d and the highest K_a are observed for highly substituted derivatives (HAC16H and HAC18H). This finding is expected, given the significant hydrophobization of these systems. For the HACxL polymers, the K_d coefficient values are similar (the same as K_a coefficient values), indicating that the length of the hydrophobic domains does not significantly affect KGN complexation in the hydrophobic core. These trends are consistent with variations in alkyl chain length and DS and correlate with the observed aggregation behavior and release profiles. Parameters such as apparent K_d and K_a, although not absolute thermodynamic constants, are widely used in the characterization of drug delivery systems to compare relative drug-carrier interactions, as they reflect the strength of partitioning into carrier domains and can inform on drug retention versus availability in biological environments [40,41]. Such an approach is very common in pharmaceutical development to deliver and/or protect active substances in drugs. However, quantitative K_a and K_d values for KGN-carrier interactions have not been reported in the literature so far. Nevertheless,

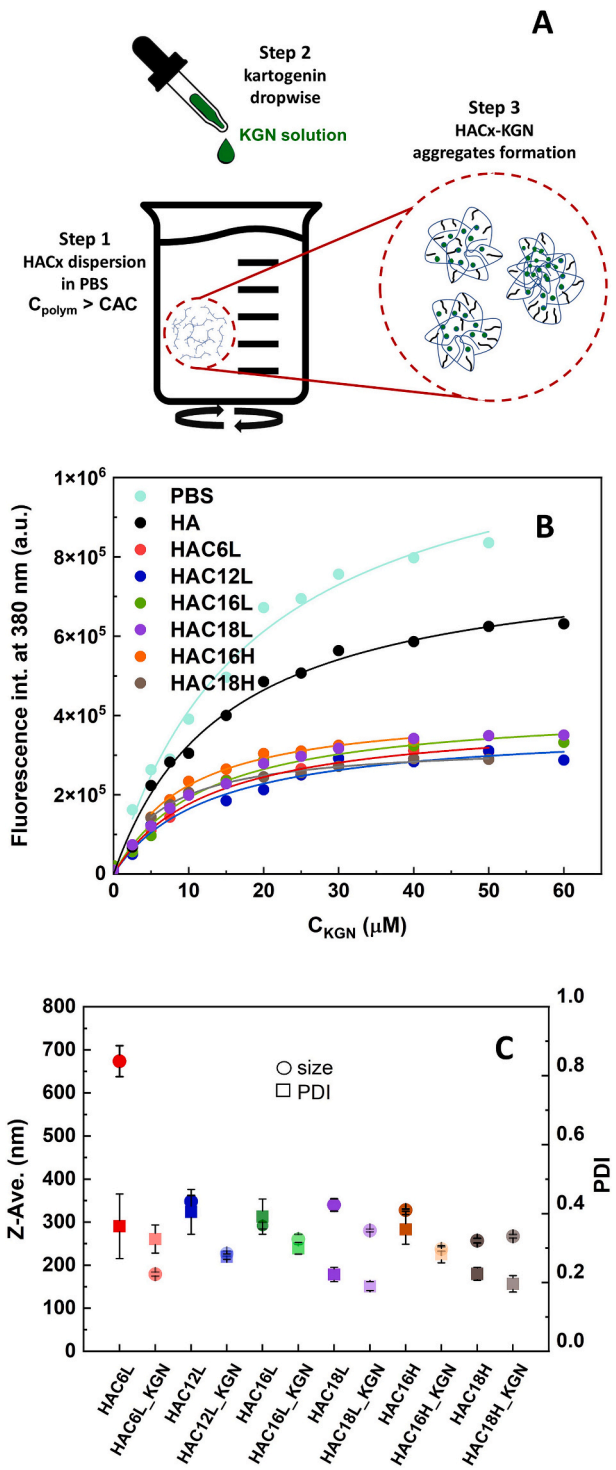

Fig. 3. Scheme of formation of HACx-KGN (A). Saturation curves for encapsulating KGN in HACx aggregates (B). Size and PDI of pure HACx and HACx-KGN aggregates at the concentration of 2 mg/mL (C).

the obtained K_a and K_d values should be interpreted as relative parameters, suitable only for comparison within the investigated HACx series under identical experimental conditions.

The self-assembly behavior of HACx polymers into nanometer-sized structures was investigated using dynamic light scattering (DLS) with a Zetasizer, both in the absence and presence of KGN, as shown in Fig. 3C. The results revealed that, in nearly all cases, the incorporation of KGN reduced both the hydrodynamic diameter and the polydispersity index

Table 2
Calculated values of K_d and K_a for KGN in free form, in the presence of HA and HACx.

Polymer	K_d (μM)	K_a (μM^{-1})
-	18.9 ± 2.7	0.054 ± 0.008
HA	15.9 ± 1.5	0.063 ± 0.006
HAC6L	12.7 ± 1.8	0.080 ± 0.011
HAC12L	12.3 ± 2.4	0.083 ± 0.015
HAC16L	12.0 ± 2.0	0.085 ± 0.014
HAC18L	12.2 ± 0.8	0.082 ± 0.005
HAC16H	8.8 ± 0.8	0.115 ± 0.011
HAC18H	6.5 ± 0.4	0.154 ± 0.009

(PDI) of the resulting polymeric aggregates relative to the free polymers. Overall, KGN incorporation yielded aggregate sizes of approximately 200–300 nm, suggesting that the drug not only exerts therapeutic effects but also contributes to the stabilization and compaction of the polymer assemblies [42]. The extent of size reduction upon KGN loading was dependent on polymer structure, with decreases of approximately 70% for HAC6L, 30% for HAC12L, 10% for HAC16L, 20% for HAC16H, and 30% for HAC18L. This trend suggests that KGN may act as a stabilizing agent during self-assembly by promoting hydrophobic interactions within the polymer aggregates. In contrast, HAC18H represented a notable exception, as its aggregate size and PDI remained comparable with and without KGN, indicating an intrinsic ability to form optimized and stable nanostructures. This behavior likely arises from a favorable hydrophobic–hydrophilic balance in HAC18H, making its self-assembly less dependent on external modulators such as drug molecules. From an application perspective, although smaller carriers (<100 nm) may penetrate deeper into cartilage due to the dense extracellular matrix, assemblies in the 200–300 nm range are commonly reported for intra-articular delivery, where prolonged joint retention and sustained local drug release are preferred [43,44]. Moreover, HA is a natural ligand for the CD44 receptor, and HA-based carriers can undergo receptor-mediated interactions that facilitate cellular association and uptake despite larger aggregate sizes [45]. Accordingly, the observed size range is consistent with the intended use of the HACx systems as local intra-articular drug reservoirs rather than deep-penetrating nanocarriers.

Moreover, the ζ-potential measurements were performed to assess whether KGN incorporation alters the surface electrokinetic properties of alkylated HA aggregates (Fig. S7). All HACx systems exhibited moderately negative ζ-potential values, consistent with the anionic nature of HA. Importantly, KGN loading induced measurable shifts in ζ-potential for several formulations, including HAC16H, HAC18L and HAC18H, indicating drug-induced reorganization of polymer aggregates rather than changes in intrinsic chemical charge. In soft, hydrated polymer assemblies, ζ-potential is highly sensitive to aggregate compaction, hydration layer thickness, and exposure of charged groups at the particle interface.

Cryo-TEM was applied to selected samples only to qualitatively visualize polymer aggregation, serving as a complementary technique to DLS and CAC analyses rather than a systematic size-quantification

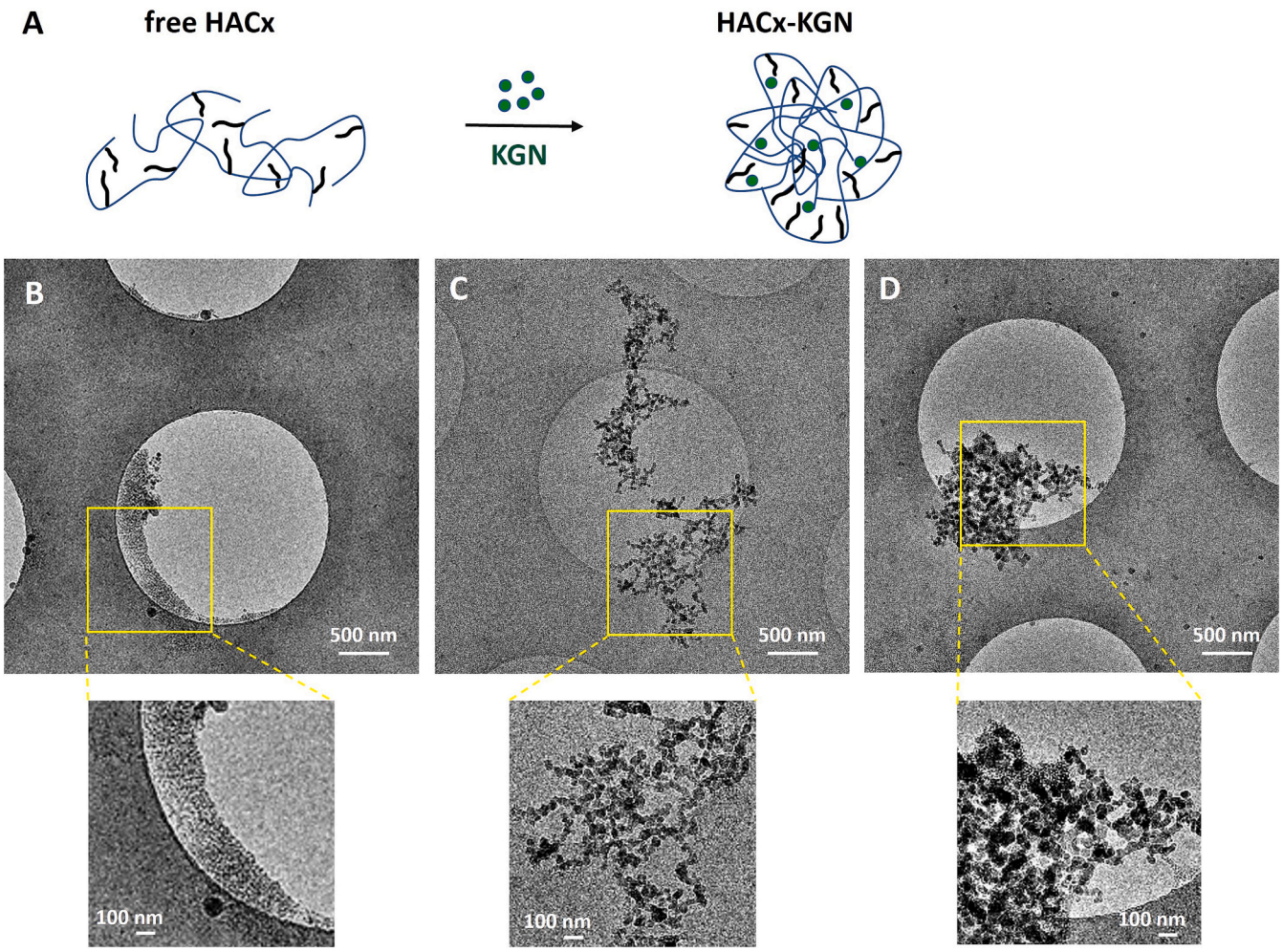

Fig. 4. Schematic illustration of aggregate formation from HACx in the presence of KGN (A). Cryo-TEM micrographs of structures formed in aqueous dispersions of HAC18L (B), HAC18L-KGN (C), and HAC12L-KGN (D) at concentrations above the CAC of the polymers.

method. The morphology of aggregates formed by the selected HACx was schematically presented and visualized using cryo-TEM (Fig. 4).

In the first step, an optimal concentration of 2 mg/mL was chosen for imaging aggregates using cryo-TEM. Afterwards, the HAC18L polymer, whose CAC is 20-times lower than the selected concentration (0.09 ± 0.01 mg/mL vs. 2 mg/mL), was imaged both without and with KGN (Fig. 4B,C). Additionally, HAC12L complexed with KGN was imaged at twice its CAC concentration (0.92 ± 0.16 mg/mL) (Fig. 4D). In all cases, individual polymer chains and/or single aggregates are not visible. For free HAC18L, the material appears as faint, tiny clusters along the edges of the grid holes, without forming a continuous or condensed network (Fig. 4B). Overall, the structure appears diffuse and loosely organized. The absence of distinct dense regions suggests that the polymer chains mostly remain separated, with minimal intermolecular interactions. Unlike free HAC18L, HAC18L-KGN aggregates show clear, dark accumulations indicating strong condensation, where the darkest objects form clusters smaller than 100 nm (Fig. 4C). DLS measurements indicated that the hydrodynamic diameter of HAC18L-KGN aggregates is around 150 nm. These assemblies form continuous chains or larger agglomerates, reflecting significant intermolecular interactions upon complexation with KGN. Compared to the free polymer, the complexed sample exhibits higher contrast and a more organized aggregation pattern, emphasizing the stabilizing and associative effects of HAC18L-KGN formation. Despite visualizing HAC12L-KGN at the polymer's CAC, the presence of KGN enhanced aggregation (Fig. 4D). Dense, high-contrast accumulations are observed, covering larger areas of the grid. The aggregates are more abundant and more compact than those formed by HAC18L-KGN. The size of individual black aggregates exceeds 100 nm, aligning with DLS data indicating a hydrodynamic diameter of approximately 200 nm for HAC12L-KGN. It is important to note that HA is difficult to visualize at high resolution using cryo-TEM without stabilization (e.g., with proteins) due to its flexible and amorphous nature [46–48]. In our previous work, we demonstrated cryo-TEM visualization of alkylated chondroitin sulfate clusters [30]. Unlike HAC18L, CSC18L formed irregular objects and rod-like particles. The CSC18L-curcumin complex formed small globular micelles that assembled into larger irregular clusters, closely resembling those formed by HACx-KGN.

Spectrofluorometric measurements were conducted to assess the release of KGN from polymer aggregates into PBS at specific time points (Fig. 5). The drug release profiles of the prepared nanocarriers (from HAC6 to HAC18) were analyzed using the Weibull statistical distribution function to gain mechanistic insight into their release behavior [49]. This model has been widely used to characterize the kinetics of various heterogeneous systems [50]. Lachowicz et al. demonstrated that the Weibull model provides the most accurate drug (piroxicam) release parameters for polysaccharide coacervates compared to other models [51].

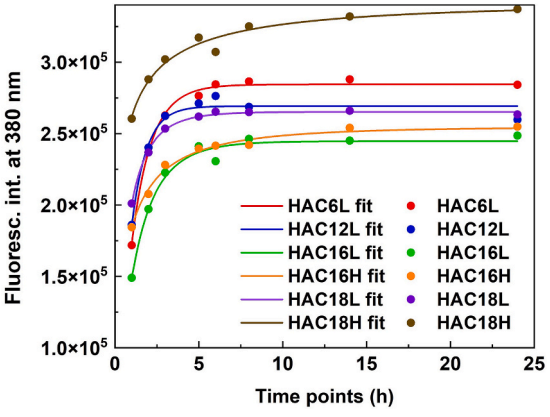

Fig. 5. Fluorescence intensity of released KGN into PBS after dialysis from HACx aggregates at specific time points (1, 2, 3, 5, 6, 8, 14, and 24 h).

The Weibull model yields the α (scale) and β (shape) parameters that describe the release profile's kinetics (Table 3). The time scale of the release curve is determined by α. As α increases, the drug's release occurs faster [52]. The lower α in the HAC18H sample suggests a maximum delay and potential suitability for long-acting systems. The β parameter indicates the mechanism by which the drug is transported through the polymer matrix and therefore serves as the shape factor describing the release profile. Estimates for $\beta \leq 0.75$ suggest Fickian diffusion in either fractal or Euclidean spaces, while a combined mechanism (Fickian diffusion and Case II transport) correlates with β values in the range $0.75 < \beta < 1$. Values exceeding 1 correspond to more complex release behavior [32,52]. Analysis of Weibull parameters revealed distinct differences in drug release kinetics among the tested formulations. HAC6L, HAC12L, and HAC16L exhibited high α values (~1.0), indicating complete release, with β values close to 1, consistent with a combined Fickian and matrix-based (Case II) transport mechanism. Conversely, HAC16H, HAC18L, and especially HAC18H displayed lower α values ($\leq$ 0.61), indicating limited release potential. Their β values (< 0.75) suggest predominantly Fickian diffusion with minimal structural contributions. Importantly, incomplete or sustained release observed for highly substituted systems should not be interpreted as a drawback. In the context of intra-articular therapy and cartilage regeneration, prolonged local availability of KGN is often advantageous, as sustained exposure at low concentrations has been shown to support chondrogenic differentiation [43,44]. The lowest values observed for HAC18H ($\alpha = 0.32 \pm 0.08$, $\beta = 0.33 \pm 0.07$) indicate a rapid, diffusion-controlled release with a steep initial phase and incomplete long-term release. Fluorescence measurements performed after 80 h and 144 h of continuous dialysis further confirmed that a significant fraction of KGN remained entrapped within the HACx assemblies (Fig. S8), supporting the concept of sustained local drug presentation rather than complete release under static in vitro conditions. Taken together, these results demonstrate that systematic tuning of hydrophobic substitution enables control over KGN release kinetics, defining a biologically relevant design space in which formulations can be selected to favor either faster drug availability or prolonged intra-articular retention, depending on therapeutic requirements.

3.3. *hUC-MSC response to HACx and their aggregates with KGN*

The cytotoxicity of HACx was evaluated and compared in both its native form and when combined with KGN on hUC-MSCs, based on the concentrations of the tested systems (Fig. 6). The IC_{50} values were calculated and are shown in Table 4.

For HAC6L, HAC12L, and HAC16L (Fig. 6A-C), only a slight reduction in cell viability was detected across all tested doses. In contrast, substantial cytotoxicity occurred in HAC16H and HAC18H at 50 μg/mL (Fig. 6D,F). In HAC18L, a concentration-dependent decline was observed at medium to high doses (Fig. 6E). The most pronounced effects were found in HAC18L and HAC18H at higher polymer levels, where viability dropped to around 20% compared to the untreated control. These results were consistent with morphological changes in cell shape and density (Fig. S9). Incorporating KGN into the polymer formulations consistently improved cell viability across several groups. Statistically significant differences between HACx and HACx-KGN conditions were noted for HAC6L, HAC16L, HAC16H, HAC18L, and HAC18H. For example, in the HAC18L group at 200 μg/mL, viability was 20.1% without KGN and 69.4% with KGN; at 150 μg/mL, the respective values were 30.2% and 79.1%. The protective effect of KGN was especially marked in the HAC18L and HAC16L systems. This benefit may be linked to polymer rearrangement in the presence of KGN, potentially altering the exposure or spatial distribution of hydrophobic domains. Previous work with alkylated chondroitin sulfate has shown that self-assembly into lipid structures reduces toxicity by limiting contact between hydrophobic polymer regions and cell membranes [38]. A similar mechanism may explain the enhanced compatibility of

Table 3
Weibull model parameters and interpretation of KGN release profiles.

Polymer	α ± SD (scale)	β ± SD (shape)	R^2	Release mechanism	Interpretation
HAC6L	1.07 ± 0.03	0.94 ± 0.05	0.9965	Mixed	Nearly complete release; combined Fickian and structural transport
HAC12L	0.86 ± 0.07	0.99 ± 0.16	0.9591	Mixed	Moderate release; close to exponential profile
HAC16L	1.08 ± 0.10	0.81 ± 0.12	0.9674	Mixed	Controlled release with dominant diffusion
HAC18L	0.61 ± 0.03	0.70 ± 0.04	0.9950	Fickian diffusion	Fast release without matrix restructuring
HAC16H	0.59 ± 0.06	0.46 ± 0.05	0.9811	Fickian diffusion	Partial release; rapid diffusion-driven profile
HAC18H	0.32 ± 0.08	0.33 ± 0.07	0.9489	Strongly Fickian diffusion	Incomplete release; rapid initial burst, purely diffusion-based

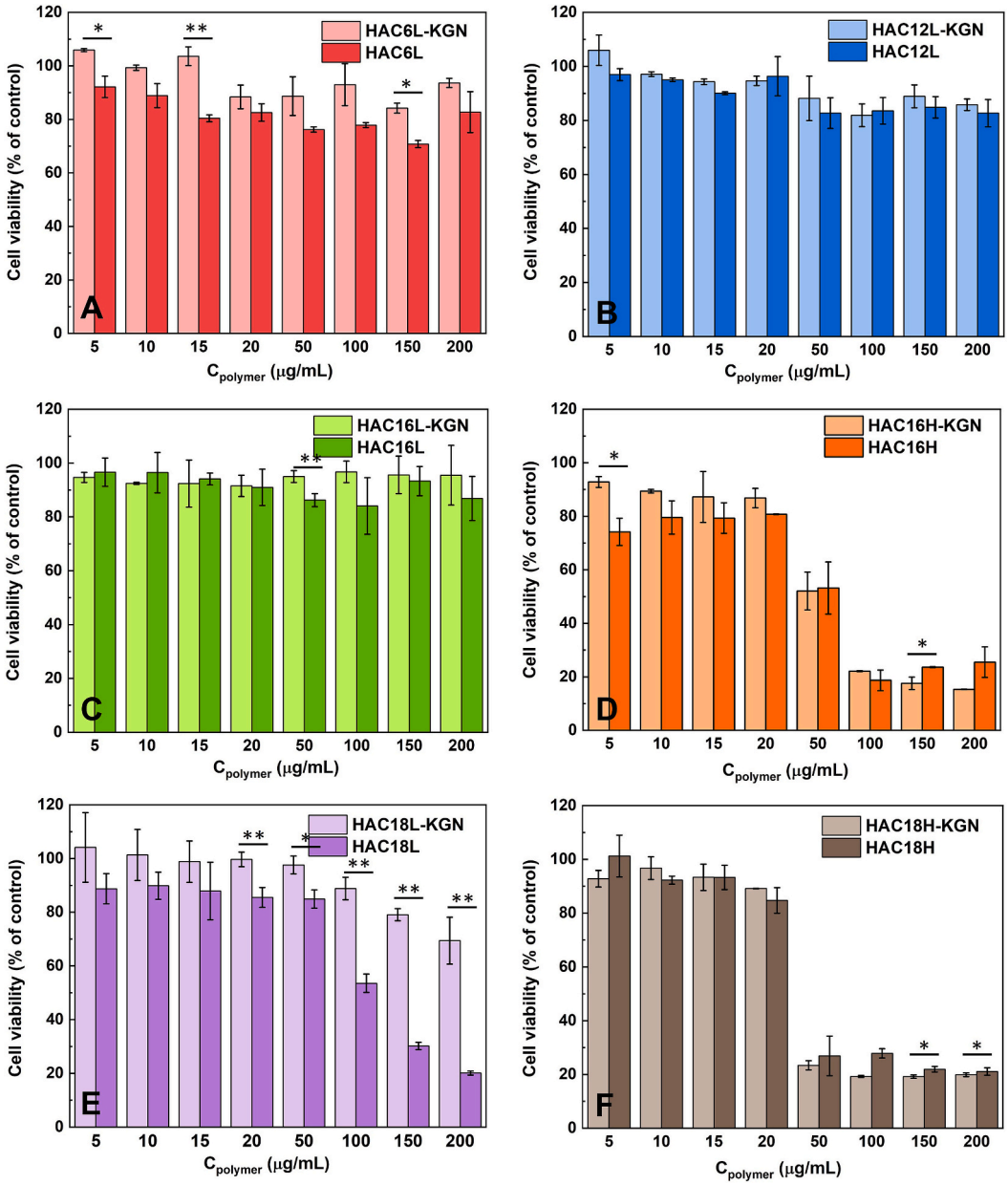

Fig. 6. Cytotoxic effect on hUC-MSCs after 24 h exposure to HAC6L with and without KGN (A), HAC12L with and without KGN (B), HAC16L with and without KGN (C), HAC16H with and without KGN (D), HAC18L with and without KGN (E), and HAC18H with and without KGN (F), measured by MTT assay. The results were normalized to the untreated control. Mean values marked with ** or * indicate significant differences (**$p < 0.01$; *$p < 0.05$) between the marked groups.

KGN-loaded formulations. The observed ζ-potential shifts upon KGN loading are therefore consistent with partial shielding of hydrophobic domains and increased surface exposure of carboxylate groups, providing experimental support for reduced membrane perturbation and improved cell viability observed for KGN-loaded systems. Taken together, the observed cytotoxicity of highly substituted derivatives indicates that HAC16H and HAC18H define the upper limits of hydrophobic modification and are not suitable for direct clinical application, whereas formulations with lower substitution levels represent more promising candidates for translational development.

Table 4
The IC_{50} values (incubation time was 24 h) assessed against hUC-MSCs for the studied polymers with and without KGN.

Polymer	IC_{50} (μg/mL) without KGN	IC_{50} (μg/mL) with KGN
HAC6L	>200	>200
HAC12L	>200	>200
HAC16L	>200	>200
HAC18L	~107	>200
HAC16H	~55	~55
HAC18H	~38	~38

3.4. Analysis of gene expression associated with chondrogenic differentiation

The expression of early (*SOX9*) and late (*ACAN* and *COL2A1*) chondrogenic markers was evaluated in response to KGN exposure in both monolayer (2D) and three-dimensional (3D) cultures. *COL1A1* was used as a marker for non-cartilaginous matrix, indicating either a fibroblastic or osteoblastic phenotype. Firstly, the effect of exposure to different concentrations of the HACx and HACx-KGN systems for 24 h was tested in the 2D model to perform a concentration screening (Fig. 7). We analyzed only non-toxic variants, specifically HAC6L and HAC12L at concentrations ranging from 5 to 100 μg/mL, and HAC16L and HAC18L at concentrations ranging from 5 to 25 μg/mL. Cytotoxic carriers such as HAC16H and HAC18H were excluded from the study. Free HAC6L upregulated the expression of chondrogenic genes *SOX9*, *ACAN* and *COL2A1* at concentrations between 25 and 100 μg/mL, while it did not significantly affect *COL1A1* (Fig. 7A-D). The lowest concentration of HAC16L increased *SOX9* and *COL2A1* but failed to increase *ACAN* while HAC12L and HAC18L did not influence chondrogenesis of hUC-MSCs in 2D culture (Fig. 7A-D). For HACx-KGN aggregates, an apparent increase in the expression of all three chondrogenic markers was observed only in HAC18L-KGN (Fig. 7A'-D'). Interestingly, HAC12L-KGN at doses between 5 and 10 μg/mL significantly increased *COL2A1* (Fig. 7C') but not *SOX9* or *ACAN*. *COL1A1* expression peaked in HAC6L-KGN at 100 μg/mL (7.8-fold), while in other conditions it was not significantly affected (Fig. 7D').

To directly address the translational relevance of the carrier system, free KGN was included as an additional control under equivalent experimental conditions (Fig. S10). Soluble KGN induced chondrogenic marker expression at concentrations of 0.25 μM and higher. At 0.25 μM, significant induction of *ACAN* (5.35-fold) and *SOX9* (4.64-fold) was observed, whereas *COL2A1* upregulation became more pronounced at 0.375 μM (6.90 ± 0.61-fold) and further increased at 0.5 μM (8.31 ± 0.37-fold). In contrast, HAC12L-KGN elicited robust *COL2A1* upregulation (approximately 7–12-fold) within the lower concentration range of 5–10 μg/mL polymer, corresponding to substantially lower effective KGN doses. These results indicate that the amphiphilic HA carriers preserve KGN bioactivity while modulating its effective transcriptional response profile. The formulation-dependent differences suggest that biological performance is closely associated with alkyl modification patterns and release behavior rather than absolute KGN concentration alone.

Alcian Blue with Fast Green staining performed after 7 days of 2D culture showed detectable glycosaminoglycan-associated staining in cells treated with HAC12L-KGN (25 μg/mL polymer; 0.125 μM KGN) and HAC16L-KGN (25 μg/mL polymer; 0.125 μM KGN) (Fig. S11). Compared to the control condition, treated samples displayed modest but visible Alcian-positive areas localized mainly in the pericellular regions. Fast Green staining confirmed preserved cellular morphology and comparable cell distribution. These observations indicate early extracellular matrix-associated changes under polymer-mediated KGN delivery in 2D culture.

To further assess the effect of the HACx and HACx-KGN on chondrogenesis, we used a **3D** hUC-MSC spheroid culture for three weeks and selected the concentration of 7.5 μg/mL for all formulations. This dosage was selected based on the 2D results, where the HACx-KGN elicited strong expression of key chondrogenic markers while preserving high cell viability and minimizing cytotoxicity. Moreover, we evaluated the effect of these systems both with and without TGFβ1 (2 ng/mL) to generate a more chondrogenic permissive condition.

Without TGFβ1, HAC6L-KGN and HAC16L-KGN markedly upregulated *SOX9*, *ACAN*, and *COL2A1* relative to the untreated control, with the strongest effects observed for HAC16L-KGN (*SOX9*: 18.7-fold, *ACAN*: 9.5-fold, *COL2A1*: 40.8-fold) (Fig. 8). Although the corresponding KGN-free systems (HAC6L and HAC16L) also exhibited elevated expression levels compared to the control, the magnitude of these changes was substantially lower, indicating a more pronounced chondrogenic response in the presence of KGN (Fig. 8). HAC18L and HAC12L did not significantly affect the expression of chondrogenic marker genes, with nor without KGN (Fig. 8). Under more chondrogenesis stimulating culture conditions in the presence of TGFβ1, only HAC12L-KGN induced an upregulation of *SOX9* (17.5-fold), *ACAN* (7.3-fold), and *COL2A1* (41.1-fold), while *COL1A1* was not significantly affected. These results show that HACx-KGN has the potency to stimulate chondrogenesis.

KGN has been studied in both 2D and 3D culture systems, consistently demonstrating its ability to promote chondrogenic differentiation [53,54]. Our study confirms that KGN effectively promotes chondrogenesis in both cultures; however, the specific conditions that optimize differentiation differ between the two culture systems. In 2D culture, HAC12L-KGN and particularly HAC18L-KGN induced strong chondrogenic differentiation, whereas in 3D conditions, the most notable response was observed for HAC6L and HAC16L-KGN in the absence and HAC12L-KGN in the presence of TGFβ1. These results highlight that while KGN works well in both systems, the microenvironment and spatial cell organization significantly influence differentiation, possibly by affecting mechanotransduction and cell-cell interactions. Beyond microenvironmental factors, the KGN's delivery strategy likely played a critical role in its effectiveness in both 2D and 3D conditions. Amphiphilic HA derivatives used for KGN encapsulation may not only improve its solubility but also enhance cellular uptake, prolong retention, and increase local bioavailability within the culture system. It has been shown that HA-coated liposomes facilitate receptor-mediated endocytosis via CD44, a surface receptor highly expressed on chondroprogenitor cells [55,56]. This mechanism likely contributed to the increased chondrogenic response observed under certain conditions. Furthermore, HA is known to bind ECM components such as type 2 collagen and aggrecan, potentially slowing the diffusion of KGN-laden liposomes and prolonging their local presence in 3D environments [56]. In addition to HA, the degree of alkylation in HA derivatives (C6, C12, C18) may have further influenced membrane interactions and uptake efficiency [12]. Hydrophobic substitutions are reported to enhance interaction with the cell membrane and regulate drug release kinetics [38,57,58]. This could explain why specific conditions in 2D and 3D showed stronger differentiation responses, as variations in C6, C12, C16, and C18 likely modulated KGN availability at the cellular level. The observed differences likely reflect distinct KGN release kinetics and carrier-cell interactions modulated by alkyl chain length. According to Weibull model analysis, HAC6L and HAC12L enabled faster and more complete KGN release ($\alpha \approx 1.0$), which may be particularly beneficial in 3D cultures where dense matrices impede diffusion. In contrast, carriers such as HAC18L showed limited release ($\alpha = 0.61 \pm 0.03$; $\beta = 0.70 \pm 0.04$), potentially restricting KGN availability in 3D environments. Similar effects have been reported in other systems, where the balance between hydrophobicity and release behavior significantly influenced drug delivery efficiency and biological response in 3D conditions [59]. Sustained local release of KGN has also been shown to support chondrogenic differentiation in hydrogel-based platforms [60]. These results suggest that while KGN retains its

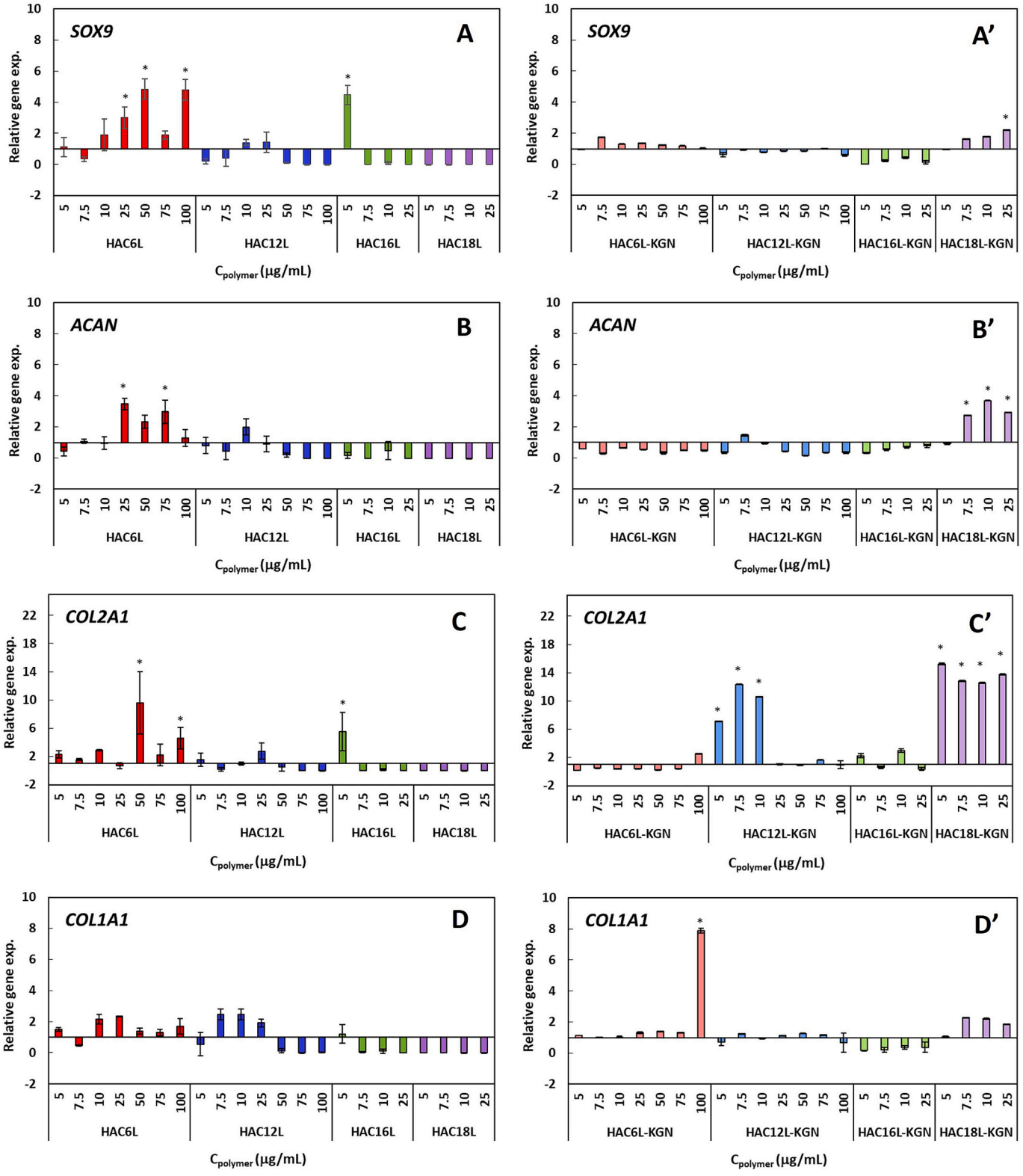

Figure 7. The expression of selected genes in hUC-MSCs cultured in 2D exposed for 24 h to pure polymers HACx (intensive color bars - A-D) vs HACx-KGN (bright color bars – A'-D'). Chondrogenic markers (*SOX9* – A, A', *ACAN* – B, B', *COL2A1* – C, C') and a non-chondrogenic marker (negative control – *COL1A1* – D, D') are presented as expression levels calculated using internal control genes *GAPDH* and *18S rRNA*, and normalized to untreated control cells. Mean values marked with * indicate statistically significant differences (*$p < 0.05$ vs untreated cells).

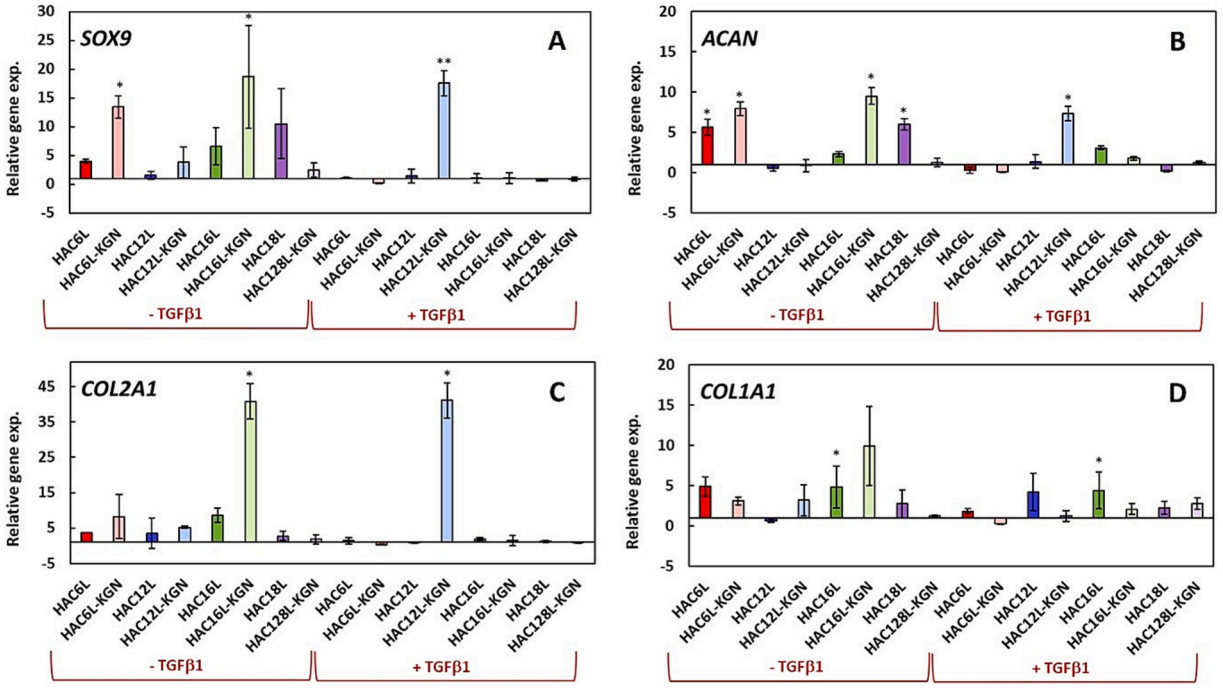

Fig. 8. Expression of selected genes in hUC-MSC spheroids cultured for 21 days with pure polymers HACx (intensive color bars) or HACx-KGN (bright color bars), both without and with TGFβ1. Chondrogenic markers (*SOX9* - A, *ACAN* - B, *COL2A1* - C) and a non-chondrogenic marker (negative control – *COL1A1* - D) are presented as expression levels using the internal control genes *GAPDH* and *18S rRNA*, and normalized to untreated control cells. Mean values marked with ** or * indicate statistically significant differences (**$p < 0.01$; *$p < 0.05$ vs untreated cells).

chondrogenic potential in both systems, its effectiveness may depend on release dynamics and microenvironmental conditions that shape the overall cellular response. This also demonstrates the value of the array of amphiphilic HA derivative formulations in enabling the selection of the appropriate system for the specific factor to be released.

4. Conclusions

Six amphiphilic HA derivatives were successfully synthesized with tailored alkyl modification patterns, varying in chain length (C6, C12, C16, C18) and DS. Polymers with ~2% substitution represented low-substituted forms, whereas those with ~5% or ~ 10% substitution constituted highly modified derivatives. The chemical modifications were confirmed by XPS, NMR, and FTIR-ATR analyses. Additional NMR studies conducted in solvents of differing polarity further demonstrated the limitations of NMR for structural characterization of these self-assembling amphiphilic derivatives, as the dynamic exposure and restricted mobility of hydrophobic groups compromise signal clarity and interpretability.

Determination of CAC values enabled identification of the optimal polymer concentrations required for effective self-aggregation and distinguished covalent polymer–amine conjugation from simple physical mixing. Fluorescence-based analyses confirmed efficient KGN encapsulation, with the highest binding affinities observed for highly substituted derivatives (HAC16H, HAC18H). KGN release from HAC16H, HAC18L, and particularly HAC18H was limited and predominantly diffusion-controlled, indicating their behavior as sustained-release reservoirs, whereas HAC6L, HAC12L, and HAC16L exhibited faster and more complex release kinetics. KGN loading additionally reduced aggregate size to the 200–300 nm range. Cryo-TEM imaging revealed diffuse, loosely organized clusters for free HAC18L, whereas HAC12L-KGN and HAC18L-KGN formed denser, more structurally defined aggregates.

Cytotoxicity studies on stem cells demonstrated that KGN incorporation improved the biocompatibility of selected systems, notably HAC16H and HAC18L. Short-term 2D cultures indicated chondrogenic potential for several formulations, particularly HAC12L and HAC18L at specific concentrations, while long-term 3D spheroid cultures showed the strongest induction of chondrogenic markers for HAC16L-KGN and HAC12L-KGN in combination with TGFβ1. Highly substituted derivatives delineated the design boundaries of hydrophobically modified HA systems, whereas formulations with moderate DS emerged as the most suitable candidates for further translational investigation.

Altogether, these results demonstrate that systematic tailoring of alkyl modification patterns in HA derivatives enables fine control over self-assembly, KGN loading, release behavior, and biological responses, positioning these carriers as promising platforms for cartilage repair applications. Direct comparison with free KGN confirmed that structurally tailored HACx-KGN systems achieve chondrogenic marker activation at lower effective drug concentrations, highlighting the added value of controlled delivery over simple drug administration. Despite the promising results, several limitations of the present study should be acknowledged. The biological evaluation was primarily conducted in vitro and therefore does not fully reproduce the complex biochemical and mechanical environment of articular cartilage in vivo. Future studies will therefore focus on HACx formulations with moderate DS to further evaluate their long-term biocompatibility and therapeutic efficacy under physiologically relevant intra-articular conditions. In particular, HAC12L-KGN, HAC16L-KGN, and HAC18L-KGN will be evaluated in advanced 3D culture models, including hydrogel-based environments, complemented by protein-level and histological analyses. Upon confirmation of biocompatibility, these formulations may be further explored in vivo using focal cartilage injury models, potentially in combination with clinically established procedures such as bone marrow stimulation or microfracture to enhance mesenchymal stem cell recruitment and support cartilage regeneration.

CRediT authorship contribution statement

Magdalena Wytrwal: Writing – review & editing, Writing – original

draft, Visualization, Validation, Resources, Project administration, Methodology, Investigation, Funding acquisition, Formal analysis, Data curation, Conceptualization. **Sylwia Rzepa:** Writing – review & editing, Writing – original draft, Visualization, Project administration, Investigation. **Ewa Ocłoń:** Writing – original draft, Formal analysis. **Mirosław Kucharski:** Investigation, Data curation. **Ewelina Bik:** Investigation. **Katarzyna Filipek:** Investigation. **Wendy Koevoet:** Methodology, Investigation. **Gerjo J.V.M. van Osch:** Writing – review & editing, Writing – original draft, Supervision, Methodology. **Szczepan Zapotoczny:** Writing – review & editing, Supervision.

Declaration of competing interest

The authors declare that they have no known competing financial interests or personal relationships that could have appeared to influence the work reported in this paper.

Acknowledgments

The research project was supported by the program "Excellence Initiative – research university" at AGH University of Krakow. The cryo-TEM micrographs were collected at the Cryo-EM Centre of the National Synchrotron Radiation Centre SOLARIS (Krakow, Poland).

Appendix A. Supplementary data

Supplementary data to this article can be found online at https://doi.org/10.1016/j.ijbiomac.2026.151809.

Data availability

Data will be made available on request.

References

[1] J.D. Steinmetz, G.T. Culbreth, L.M. Haile, et al., Global, regional, and national burden of osteoarthritis, 1990–2020 and projections to 2050: a systematic analysis for the Global Burden of Disease Study 2021, Lancet Rheumatol. 5 (9) (2023) e508–e522, https://doi.org/10.1016/s2665-9913(23)00163-7.
[2] R. Mohammadinejad, M. Ashrafizadeh, A. Pardakhty, et al., Nanotechnological strategies for osteoarthritis diagnosis, monitoring, clinical management, and regenerative medicine: recent advances and future opportunities, Curr. Rheumatol. Rep. 22 (4) (2020) 12, https://doi.org/10.1007/s11926-020-0884-z.
[3] A. Cardoneanu, L.A. Macovei, A.M. Burlui, et al., Temporomandibular joint osteoarthritis: pathogenic mechanisms involving the cartilage and subchondral bone, and potential therapeutic strategies for joint regeneration, Int. J. Mol. Sci. 24 (1) (2022) 171, https://doi.org/10.3390/ijms24010171.
[4] C. Yu, L. Li, D. Liang, et al., Glycosaminoglycan-based injectable hydrogels with multi-functions in the alleviation of osteoarthritis, Carbohydr. Polym. 290 (2022) 119492, https://doi.org/10.1016/j.carbpol.2022.119492.
[5] A. Gobbi, J.G. Lane, M. Morales, et al., Articular cartilage delamination at eight years following cellular-based repair procedures: a case reports, J. Exp. Orthop. 9 (1) (2022), https://doi.org/10.1186/s40634-022-00527-2.
[6] A. Barreto, T.R. Braun, A new treatment for knee osteoarthritis: Clinical evidence for the efficacy of Arthrokinex™ autologous conditioned serum, J. Orthop. 14 (1) (2017) 4–9, https://doi.org/10.1016/j.jor.2016.10.008.
[7] H. An, M. Zhang, Z. Gu, et al., Advances in polysaccharides for cartilage tissue engineering repair: a review, Biomacromolecules 25 (4) (2024) 2243–2260, https://doi.org/10.1021/acs.biomac.3c01424.
[8] M. Jin, J. Shi, W. Zhu, et al., Polysaccharide-based biomaterials in tissue engineering: a review, Tissue Eng. Part B Rev. 27 (6) (2021) 604–626, https://doi.org/10.1089/ten.TEB.2020.0208.
[9] M.M.H. Rumon, A.A. Akib, S.D. Sarkar, et al., Polysaccharide-based hydrogels for advanced biomedical engineering applications, ACS Polym. Au 4 (6) (2024) 463–486, https://doi.org/10.1021/acspolymersau.4c00028.
[10] L. Zhao, Y. Zhou, J. Zhang, et al., Natural polymer-based hydrogels: from polymer to biomedical applications, Pharmaceutics 15 (10) (2023) 2514, https://doi.org/10.3390/pharmaceutics15102514.
[11] M. Pavan, D. Galesso, G. Menon, et al., Hyaluronan derivatives: Alkyl chain length boosts viscoelastic behavior to depolymerization, Carbohydr. Polym. 97 (2) (2013) 321–326, https://doi.org/10.1016/j.carbpol.2013.04.090.
[12] M. Pavan, D. Galesso, C. Secchieri, et al., Hyaluronic acid alkyl derivative: A novel inhibitor of metalloproteases and hyaluronidases, Int. J. Biol. Macromol. 84 (2016) 221–226, https://doi.org/10.1016/j.ijbiomac.2015.12.003.
[13] J.R.E. Fraser, T.C. Laurent, U.B.G. Laurent, Hyaluronan: its nature, distribution, functions and turnover, J. Intern. Med. 242 (1) (1997) 27–33, https://doi.org/10.1046/j.1365-2796.1997.00170.x.
[14] E. Trenkenschuh, W. Friess, Freeze-drying of nanoparticles: how to overcome colloidal instability by formulation and process optimization, Eur. J. Pharm. Biopharm. 165 (2021) 345–360, https://doi.org/10.1016/j.ejpb.2021.05.024.
[15] S. Federico, G. Pitarresi, F.S. Palumbo, et al., Hyaluronan alkyl derivatives-based electrospun membranes for potential guided bone regeneration: fabrication, characterization and in vitro osteoinductive properties, Colloids Surf. B: Biointerfaces 197 (2021) 111438, https://doi.org/10.1016/j.colsurfb.2020.111438.
[16] I. Andreana, V. Bincoletto, M. Manzoli, et al., Freeze drying of polymer nanoparticles and liposomes exploiting different saccharide-based approaches, Materials 16 (3) (2023) 1212, https://doi.org/10.3390/ma16031212.
[17] J. Szafraniec, A. Błażejczyk, E. Kus, et al., Robust oil-core nanocapsules with hyaluronate-based shells as promising nanovehicles for lipophilic compounds, Nanoscale 9 (47) (2017) 18867–18880, https://doi.org/10.1039/C7NR05851A.
[18] W.M. Payne, D. Svechkarev, A. Kyrychenko, et al., The role of hydrophobic modification on hyaluronic acid dynamics and self-assembly, Carbohydr. Polym. 182 (2018) 132–141, https://doi.org/10.1016/j.carbpol.2017.10.054.
[19] M. Chernos, D. Grecov, E. Kwok, et al., Rheological study of hyaluronic acid derivatives, Biomed. Eng. Lett. 7 (1) (2017) 17–24, https://doi.org/10.1007/s13534-017-0010-y.
[20] W.N. Zeng, Y. Zhang, D. Wang, et al., Intra-articular injection of kartogenin-enhanced bone marrow-derived mesenchymal stem cells in the treatment of knee osteoarthritis in a rat model, Am. J. Sports Med. 49 (10) (2021) 2795–2809, https://doi.org/10.1177/03635465211023183.
[21] J. Yang, Y. Zhu, F. Wang, et al., Microfluidic liposomes-anchored microgels as extended delivery platform for treatment of osteoarthritis, Chem. Eng. J. 400 (2020) 126004, https://doi.org/10.1016/j.cej.2020.126004.
[22] A. Xie, J. Xue, Y. Wang, et al., Kartogenin induced adipose-derived stem cell exosomes enhance the chondrogenic differentiation ability of adipose-derived stem cells, Dis. Markers 2022 (2022) 1–14, https://doi.org/10.1155/2022/6943630.
[23] C. Yu, D. Li, C. Wang, et al., Injectable kartogenin and apocynin loaded micelle enhances the alleviation of intervertebral disc degeneration by adipose-derived stem cell, Bioact. Mater. 6 (10) (2021) 3568–3579, https://doi.org/10.1016/j.bioactmat.2021.03.018.
[24] L. Cui, Z. Yang, J. Hong, et al., Injectable and degradable POSS–polyphosphate–polysaccharide hybrid hydrogel scaffold for cartilage regeneration, ACS Appl. Mater. Interfaces 15 (17) (2023) 20625–20637, https://doi.org/10.1021/acsami.2c22947.
[25] C. Huang, G. Zhong, J. Xiao, et al., An injectable kartogenin-incorporated hydrogel supports mesenchymal stem cells for cartilage tissue engineering, Bioengineering 12 (5) (2025) 434, https://doi.org/10.3390/bioengineering12050434.
[26] M.-L. Kang, S.-Y. Jeong, G.-I. Im, Hyaluronic Acid Hydrogel Functionalized with Self-Assembled Micelles of Amphiphilic PEGylated Kartogenin for the Treatment of Osteoarthritis, Tissue Eng. Part A 23 (13–14) (2017) 630–639, https://doi.org/10.1089/ten.tea.2016.0524.
[27] P. Tikakosol, P.D. Topham, M.J. Derry, et al., Kartogenin-encapsulated self-healing injectable hydrogel based on hyaluronic acid and chitosan derivative for use as viscosupplementation in knee osteoarthritis, Int. J. Biol. Macromol. 328 (2025) 147304, https://doi.org/10.1016/j.ijbiomac.2025.147304.
[28] G. Li, R. Ni, Z. Shi, et al., Enhancing BMSC chondrogenesis with a dynamic viscoelastic hyaluronan hydrogel loaded with kartogenin for cartilage repair, Int. J. Biol. Macromol. 312 (2025) 144042, https://doi.org/10.1016/j.ijbiomac.2025.144042.
[29] N. Toriyabe, Y. Hayashi, M. Hyodo, et al., Synthesis and evaluation of stearylated hyaluronic acid for the active delivery of liposomes to liver endothelial cells, Biol. Pharm. Bull. 34 (7) (2011) 1084–1089, https://doi.org/10.1248/bpb.34.1084.
[30] A. Żak, G. Łazarski, M. Wytrwal-Sarna, et al., Molecular insights into the self-assembly of hydrophobically modified chondroitin sulfate in aqueous media, Carbohydr. Polym. 297 (2022) 119999, https://doi.org/10.1016/j.carbpol.2022.119999.
[31] L.A. Prieto-Costas, L. Milton, C.M. Quiñones-Jurgensen, et al., Screening and quantification of the encapsulation of dyes in supramolecular particles, Langmuir 37 (43) (2021) 12681–12689, https://doi.org/10.1021/acs.langmuir.1c02065.
[32] C. Corsaro, G. Neri, A.M. Mezzasalma, et al., Weibull modeling of controlled drug release from Ag-PMA nanosystems, Polymers 13 (17) (2021) 2897, https://doi.org/10.3390/polym13172897.
[33] R. Narcisi, W.J.L.M. Koevoet, G.J.V.M. van Osch, Expansion and chondrogenic differentiation of human bone marrow-derived mesenchymal stromal cells, Methods Mol. Biol. 2221 (2021) 15–28, https://doi.org/10.1007/978-1-0716-0989-7_2.
[34] P. Chomczynski, N. Sacchi, Single-step method of RNA isolation by acid guanidinium thiocyanate-phenol-chloroform extraction, Anal. Biochem. 162 (1) (1987) 156–159, https://doi.org/10.1006/abio.1987.9999.
[35] M.W. Pfaffl, A new mathematical model for relative quantification in real-time RT–PCR, Nucleic Acids Res. 29 (9) (2001) 2001–2007, https://doi.org/10.1093/nar/29.9.e45.
[36] V. Malytskyi, J. Moreau, M. Callewaert, et al., Synthesis and characterization of conjugated hyaluronic acids. Application to stability studies of chitosan-hyaluronic acid nanogels based on fluorescence resonance energy transfer, Gels 8 (3) (2022) 182, https://doi.org/10.3390/gels8030182.
[37] A. Chattopadhyay, E. London, Fluorimetric Determination of Critical Micelle Concentration Avoiding Interference from Detergent Charge, Anal. Biochem. 139 (2) (1984) 408–412, https://doi.org/10.1016/0003-2697(84)90026-5.

[38] M. Wytrwal, K. Szmajnta, M. Kucharski, et al., Kartogenin-loaded liposomes coated with alkylated chondroitin sulfate for cartilage repair, Int. J. Pharm. 646 (2023) 123436, https://doi.org/10.1016/j.ijpharm.2023.123436.
[39] C. Albrecht, Joseph R. Lakowicz, Principles of fluorescence spectroscopy, 3rd edition, Anal. Bioanal. Chem. 390 (5) (2008) 1223–1224, https://doi.org/10.1007/s00216-007-1822-x.
[40] V.P. Torchilin, Multifunctional nanocarriers, Adv. Drug Deliv. Rev. 58 (14) (2006) 1532–1555, https://doi.org/10.1016/j.addr.2006.09.009.
[41] L. Prystay, M. Gosselin, P. Banks, Determination of equilibrium dissociation constants in fluorescence polarization, J. Biomol. Screen. 6 (3) (2001) 141–150, https://doi.org/10.1177/108705710100600304.
[42] M. Sousa de Almeida, E. Susnik, B. Drasler, et al., Understanding nanoparticle endocytosis to improve targeting strategies in nanomedicine, Chem. Soc. Rev. 50 (9) (2021) 5397–5434, https://doi.org/10.1039/d0cs01127d.
[43] S. Brown, J. Pistiner, I.M. Adjei, et al., Nanoparticle properties for delivery to cartilage: the implications of disease state, synovial fluid, and off-target uptake, Mol. Pharm. 16 (2) (2019) 469–479, https://doi.org/10.1021/acs.molpharmaceut.7b00484.
[44] T. Zhao, X. Li, H. Li, et al., Advancing drug delivery to articular cartilage: From single to multiple strategies, Acta Pharm. Sin. B 13 (10) (2023) 4127–4148, https://doi.org/10.1016/j.apsb.2022.11.021.
[45] S. Salathia, M.R. Gigliobianco, C. Casadidio, et al., Hyaluronic acid-based nanosystems for CD44 mediated anti-inflammatory and antinociceptive activity, Int. J. Mol. Sci. 24 (8) (2023) 7286, https://doi.org/10.3390/ijms24087286.
[46] M.K. Cowman, S. Matsuoka, Hyaluronan and hyaluronan fragments, Carbohydr. Res. 340 (5) (2005) 791–809, https://doi.org/10.1016/j.carres.2004.11.027.
[47] O. Guvench, Atomic-resolution experimental structural biology and molecular dynamics simulations of hyaluronan and its complexes, Molecules 27 (21) (2022) 7276, https://doi.org/10.3390/molecules27217276.
[48] F.P. Maloney, J. Kuklewicz, R.A. Corey, Structure, substrate recognition and initiation of hyaluronan synthase, Nature (2022), https://doi.org/10.1038/s41586-022-04534-2.
[49] L. Kolar-Anić, S. Veljković, S. Kapor, et al., Weibull distribution and kinetics of heterogeneous processes, J. Chem. Phys. 63 (2) (1975) 663–668, https://doi.org/10.1063/1.431388.
[50] U.d.J. Martín-Camacho, N. Rodríguez-Barajas, J.A. Sánchez-Burgos, et al., Weibull β value for the discernment of drug release mechanism of PLGA particles, Int. J. Pharm. 640 (2023) 123017, https://doi.org/10.1016/j.ijpharm.2023.123017.
[51] D. Lachowicz, A. Kaczyńska, A. Bodzon-Kulakowska, et al., Coacervate thermoresponsive polysaccharide nanoparticles as delivery system for piroxicam, Int. J. Mol. Sci. 21 (24) (2020) 9664, https://doi.org/10.3390/ijms21249664.
[52] V. Papadopoulou, K. Kosmidis, M. Vlachou, et al., On the use of the Weibull function for the discernment of drug release mechanisms, Int. J. Pharm. 309 (1) (2006) 44–50, https://doi.org/10.1016/j.ijpharm.2005.10.044.
[53] C.-Y. Chen, C. Li, C.-J. Ke, et al., Kartogenin enhances chondrogenic differentiation of MSCs in 3D tri-copolymer scaffolds and the self-designed bioreactor system, Biomolecules 11 (1) (2021) 115, https://doi.org/10.3390/biom11010115.
[54] T. Spakova, J. Plsikova, D. Harvanova, et al., influence of kartogenin on chondrogenic differentiation of human bone marrow-derived MSCs in 2D culture and in co-cultivation with OA osteochondral explant, Molecules 23 (1) (2018), https://doi.org/10.3390/molecules23010181.
[55] O.K. Kari, S. Tavakoli, P. Parkkila, et al., Light-activated liposomes coated with hyaluronic acid as a potential drug delivery system, Pharmaceutics 12 (8) (2020) 763, https://doi.org/10.3390/pharmaceutics12080763.
[56] H.S.S. Qhattal, T. Hye, A. Alali, et al., Hyaluronan polymer length, grafting density, and surface poly(ethylene glycol) coating influence in vivo circulation and tumor targeting of hyaluronan-grafted liposomes, ACS Nano 8 (6) (2014) 5423–5440, https://doi.org/10.1021/nn405839n.
[57] M. Wytrwal-Sarna, P. Knobloch, S. Lasota, et al., Effect of polycation nanostructures on cell membrane permeability and toxicity, Environ. Sci. Nano 9 (2) (2022) 702–713, https://doi.org/10.1039/d1en01156a.
[58] M.R. Preiss, A. Hart, C. Kitchens, et al., Hydrophobic nanoparticles modify the thermal release behavior of liposomes, J. Phys. Chem. B 121 (19) (2017) 5040–5047, https://doi.org/10.1021/acs.jpcb.7b01702.
[59] D. Desai, M. Åkerfelt, N. Prabhakar, et al., Factors affecting intracellular delivery and release of hydrophilic versus hydrophobic cargo from mesoporous silica nanoparticles on 2D and 3D cell cultures, Pharmaceutics 10 (4) (2018) 237, https://doi.org/10.3390/pharmaceutics10040237.
[60] W. Zhang, R. Chen, X. Xu, et al., Construction of biocompatible hydrogel scaffolds with a long-term drug release for facilitating cartilage repair, Front. Pharmacol. 13 (2022), https://doi.org/10.3389/fphar.2022.922032.